Desalination and Water Treatment
www.deswater.com

doi: 10.5004/dwt.2022.28812

271 (2022) 48–57
September

Evaluation of surfactant-modified bentonite for Acid Red 88 dye adsorption in batch mode: kinetic, equilibrium, and thermodynamic studies

Aram Dokht Khatibi[a], Murat Yilmaz[b], Amir Hossein Mahvi[c], Davoud Balarak[a,*], Sabereh Salehi[d]

[a]*Department of Environmental Health, Health Promotion Research Center, Zahedan University of Medical Sciences, Zahedan, Iran, email: dbalarak2@gmail.com (D. Balarak)*

[b]*Osmaniye Korkut Ata University, Faculty of Engineering, Department of Chemical Engineering, 80000 Osmaniye, Turkey*

[c]*Department of Environmental Health Engineering, School of Public Health, Tehran University of Medical Sciences, Tehran, Iran*

[d]*Student Research Committee, Zahedan University of Medical Sciences, Zahedan, Iran*

Received 23 January 2022; Accepted 3 August 2022

ABSTRACT

In this study, hexadecyltrimethylammonium (HDTMA) bentonite was synthesized by placing alkylammonium cation onto bentonite. Acid Red 88 (AR88) removal by hexadecyltrimethylammonium (HDTMA) modified bentonite was investigated and the specific surface area obtained using Brunauer–Emmett–Teller analysis was 49.2 m^2/g for HDTMA-bentonite. However, for natural bentonite, it was only 17.4 m^2/g. The effect of main experimental parameters on the removal of AR88 (i.e., initial AR88 concentration, contact time, and HDTMA-bentonite mass) was investigated. Also, six isotherm models were applied for evaluation of the equilibrium adsorption; among the mentioned models, fitting the adsorption data on Langmuir isotherm was associated with superior results (maximum monolayer capacity (q_{max}) was 91.7 mg/g). The results gave the green light to the unique usability of the pseudo-second-order kinetics model for the portrayal of adsorption data. Using the intraparticle diffusion model, the identification of the adsorption mechanism process was done so that the trivial effect of the boundary layer was confirmed. Based on Boyd's kinetic model, the external mass transport was the foremost reason for the adsorption of water from dye–water mixtures. In addition, there is no study in the literature on the removal of Acid Red 88 dye using HDTMA-bentonite. The obtained results indicated that, through using HDTMA-bentonite, the elimination of acid dyes from aqueous solutions can occur simply and in a short time.

Keywords: Isotherms; Error function; Acid Red 88; Kinetics; HDTMA-bentonite

1. Introduction

Generating wastewater and polluting the water by it has been inscribed as a result of the accelerated development in industrialization, which has induced different concerns [1,2]. Unloading wastewater into water bodies (e.g., rivers, lakes, and oceans) without proper treatment has brought severe harmful and destructive conditions for the environment and subsequently human health [3–6].

In the industries, different kinds of dyes are employed. These dyes are also appearing in the effluents due to release from some of these industries [7–9]. Dyes are generally non-biodegradable and have good stability against light, heat, and oxidizing agents [10,11]. Dyes, through imparting color to the water bodies and coloring them, make their presence strikingly visible [12–14]. Blockage of the passage of sunlight in the dye contaminated-waters can lead to adverse effects on aquatic diversity [15,16].

* Corresponding author.

Above-mentioned issues and problems are created by releasing the generated wastewaters of industrial processes with remarkable values of dyes when discharged into the environment without any prior treatment [17,18].

Therefore, the removal of the dye is a major challenge as the treatment of such waste water by traditional treatment methods is not easily carried out and is associated with many difficulties [19,20]. These processes are usually not economically feasible and energy-efficient, especially when the color concentration is low [21]. Hence finding a suitable alternative treatment to overcome all these limitations is of great significance [22]. Although there is no doubt about the cost-effectiveness of the adsorption process for removal of dyes and treating the dye-containing effluents, its efficiency is governed by choosing the appropriate adsorbent [23,24]; so that the chosen adsorbent should exhibit some features, for example, being easily available and cheap and could accommodate the acceptance for being utilized for treatment industrial effluents [25,26].

Employing the clay mineral has undeniably gained more popularity so that it has been broadly utilized as an adsorbent for the treatment of contaminated sewage (i.e., for removal of dyes, phenolic compounds, and heavy metals) [27–29]. In addition to superb specific surface areas mentioned for these substances, they have also excellent exchange capacities; these features give their sorption capabilities to them [30,31]. Two silica tetrahedral sheets with a central Al octahedral layer consist of bentonite, which is mainly smectite clay [32]. As stated, because of its characteristics (relatively high cation exchangeability and specific surface area), the removal of contaminants using bentonite is based on ion exchange and adsorption mechanisms [33]. Nonetheless, the employment of bentonite for removing pollutants is associated with limitations since bentonite has normally a negative basal surface charge, which leads to the occurrence of poor electrostatic interactions [34]. However, the structure of this natural bentonite is not stable and can be damaged by harmful substances originated from the liquid in the process of permeation. In order to solve this problem, natural bentonite has been modified by using various chemicals, such as polyacrylate, cetyltrimethylammonium bromide (CTAB) (also called the hexadecyltrimethylammonium (HDTMA)), H_2SO_4 or NaOH, and polyethyleneimine and the obtained results demonstrated that these modifications not only improved the characterizations of natural bentonite but also increased the adsorptive efficiency [35]. However, investigation of the adsorption mechanisms onto these materials has still been limited so far. In addition, there are very few studies on the removal of dyes by HDTMA-bentonite.

Indeed, this study originated from the fact that Iran is a country having a huge source of high-quality bentonite clay [3]. However, the use of this material for removing dye from wastewater is still limited so far. Therefore, this work is of particular importance as it provides a solution to use domestic bentonites for removing dye from industrial wastewater and partially contributes to the environmental protection.

Thus, the objective of this study are listed as follows: (a) synthesizing the HDTMA-bentonite, (b) the use of HDTMA-bentonite in Acid Red 88 (AR88) dye adsorption experiments, (c) conducting extra experiments for studying the effect of parameters considered in present study (contact time, temperature, pH of solution, initial AR88 concentration, and adsorbent dosage), (d) preforming the kinetic, isotherm, and thermodynamic studies, and (e) studying the recycling and reusability of the HDTMA-bentonite.

2. Materials and methods

2.1. Materials

The AR88 dye (chemical structure: $C_{20}H_{13}N_2NaO_4S$, molar mass: 400.38 g/mol and λ_{max}: 505 nm) was supplied from Alvan Sabet Co., Iran. The chemical structure of AR88 is shown in Fig. 1. In the experiment, deionized water was taken into employment for all sample preparation processes.

2.2. Preparation of HDTMA-bentonite

Preparing the HDTMA-bentonite was done by addition of bentonite (10 g) into a hexadecyltrimethylammonium (HDTMA) solution (50 mL) of known concentration and maintaining the obtained mixture in a shaker incubator (at 30°C and 150 rpm for 24 h). After centrifugation of the mixture, the supernatant was withdrawn, and the remaining solid was comprehensively rinsed with distilled water for eliminating residual HDTMA. After placing it in an oven (at 85°C), the modified bentonite was dried. After screening by a 110 mesh sieve, it was stored in a desiccator [33].

2.3. Adsorption processes

Effects of parameters such as HDTMA-bentonite dosage (0.2–3 g/L), contact time (10–120 min), and initial AR88 concentration (10–100 mg/L) were investigated. The adsorption experiments were carried out in 250 mL conical flasks containing 100 mL AR88 ion solution at 25°C. In order to investigate the influence of initial AR88 concentrations on the removal of AR88 ions, about 1.5 g/L of freely suspended and immobilized biomass was added to various copper concentrations (10–100 mg/L) at 90 min, pH 7 and 120 rpm. The impact of contact time on the uptake of the AR88 ions was also investigated under the same conditions. At a time, interval (10–120 min), the filtrates were withdrawn. In this study, the adsorbent dose was first optimized. Then, the optimal adsorbent dose was used to perform contact

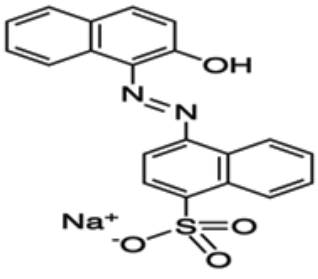

Fig. 1. Chemical structure of AR88.

time and concentration tests. Finally, the adsorbent dose, contact time and optimal dye concentration were used to perform the pH test. All tests up to this point were performed at room temperature, which was approximately 30°C. Elimination percentage and adsorption capacity are obtained from Eqs. (1) and (2) [36,37]:

$$\text{Removal efficiency}(\%) = \frac{\left(C_i - C_{\text{eq}}\right)}{C_i} \times 100 \quad (1)$$

$$q_e = \frac{V\left(C_i - C_{\text{eq}}\right)}{W} \quad (2)$$

3. Results and discussion

3.1. Characterization of HDTMA-bentonite

The specific surface area of HDTMA-bentonite was 49.2 m^2/g. The cation exchange capability (CEC) of the HDTMA-bentonite was assessed by the ethanol- ammonium chloride method; its value was detected to be 137.2 mmol/kg. As clarified in the above results, the modification with HDTMA was associated with a noteworthy development in the specific surface area and CEC (specific surface area and CEC for natural bentonite was 17.4 m^2/g and 81.3 mmol/kg).

Considering scanning electron microscopy (SEM) of bentonite and HDTMA-bentonite (Fig. 2a and b), we can observe the un-smooth surface for bentonite. However, due to the very complex surface structure on the broad plane with high micro-island frequency and ragged, broken nano-sized edges across the decreased areas of the basal plane, we could find remarkable characteristics for the adsorption of HDTMA on its surface, as detected. Moreover, obvious changes in its surface could not be distinguished after its modification by HDTMA. In addition, according to energy dispersion spectra, the presence of carbon on the bentonite surface, after modification, was approved.

3.2. Effect of different parameters on dye removal

The effect of HDTMA-bentonite mass on the AR88 removal percentage exposed in Fig. 3 was indicative of developing AR88 removal percent up to the optimal value of dosage. Using the dosage greater than the optimum value, a substantial change in percent removal was acquired. As estimated, for a given initial AR88 concentration, we observed a decrease in the equilibrium concentration by an increase in adsorbent dosage, since there will be a development in the surface area or a number of adsorption sites by increasing the adsorbent dosage [38,39].

The study was also performed using bentonite and the results showed that the optimal contact time was obtained in 150 min while the removal percentage was 76%. The higher percentage of dye removal by HDTMA-bentonite than bentonite is due to the higher specific surface area of modified bentonite and the different functional groups on the modified adsorbent surface.

The efficiency of AR88 adsorption onto HDTMA-bentonite at different contact times was investigated (Fig. 4). During the first 45 min, reasonably rapid adsorption happened, and a slower stage was detected by increasing time until attainment of equilibrium time. The removal curves are single, smooth, and continuous; this signifies that there is a probability of forming monolayer coverage of AR88 at the outer surface of the evaluated adsorbent. The results illuminate that 90 min can be selected as the equilibrium time for conducting the rest of the batch experiments. Describing the relatively high removal of AR88 is carried out based on the presence of an enormous number of vacant sites for AR88

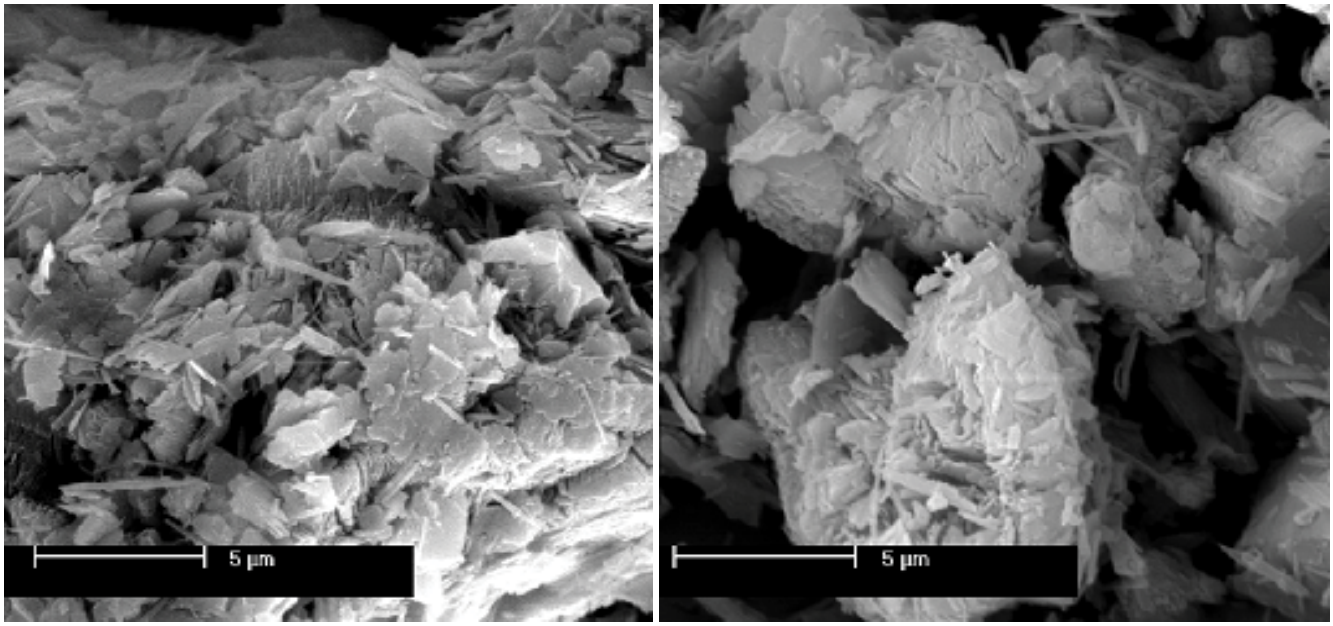

Fig. 2. SEM of bentonite and HDTMA-bentonite.

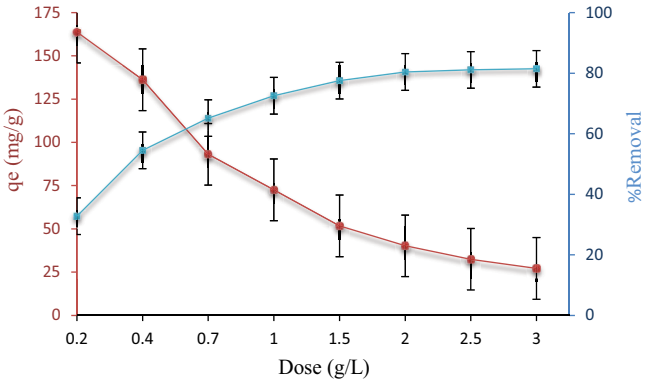

Fig. 3. Effects of adsorbent mass on the AR88 adsorption capacity and % removal (C_0 = 100 mg/L; pH = 5; time = 90 min; temperature: 30°C).

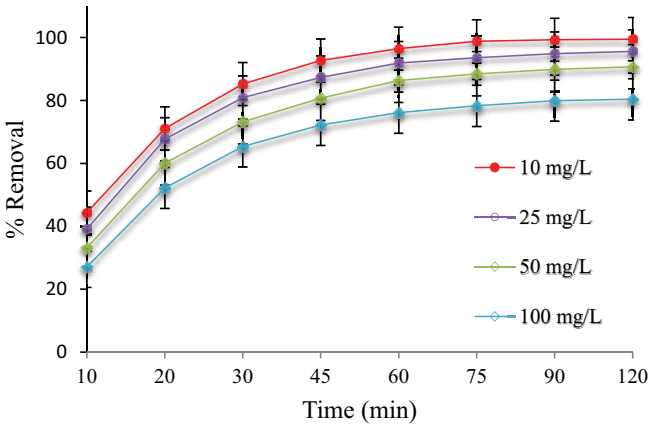

Fig. 4. Effect of dye concentration and contact time on the AR88 (adsorbent dose = 2 g/L; pH = 5; temperature: 30°C).

adsorption. However, it reaches a constant value after a while, and further removal of dye from the solution could not be observed [40].

The obtained data exhibited that as the concentration of the target pollutant was increased from 10 to 100 mg/L, an enhancement in AR88 adsorption capacity of HDTMA-bentonite from 4.975 to 40.19 mg/g was sensed, which is ascribed to a high-mass transfer force [41]. Nonetheless, the saturation of binding sites onto the HDTMA-bentonite has resulted in the diminishing AR88 percent removal from 99.5 to 80.39 (Fig. 4) [42].

The adsorption process is strongly influenced by the pH of the solution, which affects the carboxyl, hydroxyl and amino groups on the surface of the adsorbent. Determination of the equilibrium adsorbed amount of Acid Red 88 (AR88) dye (q_e) and removal of these dyes; performed at room temperature at an initial AR88 dye concentration of 10 mg/L and using 2 g/L HDTMA-bentonite as the adsorbent. The adsorption of AR88 dye was studied at pH values between 3 and 11 for 2 h and pH changes are shown in Fig. 5. For AR88 dye removal using HDTMA-bentonite, it can be seen in Fig. 5 that the highest AR88 dye removal (99.5%) occurred at pH = 3. In the AR88 dye removal study, continuously increasing the pH from 3 to 11 caused the adsorption rate to decrease from 99.5% to 49.2%. Considering the studies on azo dye removal, Khaled et al. [43], in their Direct Yellow 12 dye removal study, found that the adsorption efficiency decreased from 98.1% to 11.1% by increasing the pH of the solution from 1.5% to 11.1%. The presence of excess OH ions in a high pH solution reduces adsorption efficiency as they compete with the anions of AR88 dye, an anionic dye, for adsorption sites. In addition, the HDTMA-bentonite adsorbent aims to adsorb OH ions with high concentration and high mobility more than dye anions.

The pH value at which the adsorbent surface is electrically neutral can be determined by determining the point of zero charge (pH_{PZC}) [44]. To find out pH_{PZC}, the experiments were performed at different pH ranges from 2 to 11 using 2 g/L of adsorbent and stirred on a magnetic stirrer. As shown in Fig. 6, the pH_{PZC} of HDTMA-bentonite was determined to be 6.2. At solution pH > pH_{PZC}, the HDTMA-bentonite surface is negatively charged and electrostatic

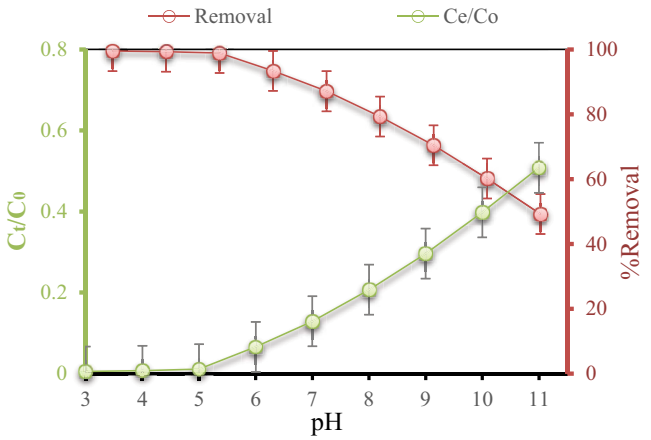

Fig. 5. Effect of pH on the AR88 removal (adsorbent dose = 2 g/L; contact time = 90 min; temperature: 30°C; C_0 = 10 mg/L).

repulsive forces form between it and negatively charged anionic dyes. The test results obtained confirm this.

3.3. Adsorption isotherms

Adsorption isotherms are valuable for optimizing the use of adsorbents. Through the fitting, of the data to different isotherm models, the analysis of the isotherm data is carried out, which is considered an imperative step for providing a competent model that can be helpful for design purposes.

3.3.1. Langmuir isotherm

Eq. (3) represents the Langmuir isotherm model (its linear form) [45,46]:

$$\frac{C_e}{q_e} = \frac{1}{q_m K_L} + \frac{C_e}{q_m} \tag{3}$$

The dimensionless equilibrium parameter 'R_L' is given as [47,48]:

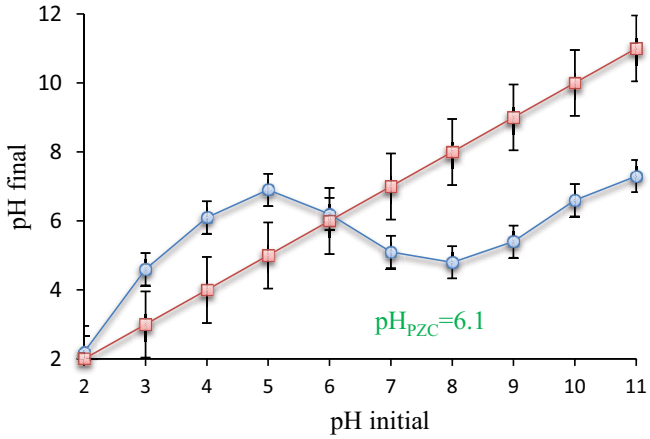

Fig. 6. Plot of pH_{final} vs. $pH_{initial}$ (AR88 dye = 10 mg/L; adsorbent = 2 g/L; temperature = 30°C).

$$R_L = \frac{1}{1 + K_L C_0} \tag{4}$$

3.3.2. Freundlich isotherm

The following equation is related to linear form of Freundlich isotherm [49,50]:

$$\log q_e = \frac{1}{n} \log C_e \log K_F \tag{5}$$

where $1/n$ points to the adsorption intensity in which for $1/n$ less than 1, the adsorption is favorable, and for its value greater than 1, the process is unfavorable.

3.3.3. Temkin isotherm

The linear Temkin equation could be given as following Eq. (6) [51]:

$$q_e = \frac{RT}{b} \ln K + \frac{RT}{b} \ln C_e \tag{6}$$

3.3.4. Harkin–Jura isotherm

The Harkin–Jura model is expressed as [52,53]:

$$\frac{1}{q_e^2} = \frac{B}{A} - \frac{1}{A} \log C_e \tag{7}$$

where A and B are Harkin–Jura constants. Harkin–Jura equation considers multilayer adsorption in terms of heterogeneity in the distribution of pores.

3.3.5. Dubinin–Radushkevich model

The linear equation of the isotherm is written as [54]:

$$\text{Log } q_e = \log q_m - \beta \varepsilon^2 \tag{8}$$

$$\varepsilon = RT \ln \left(1 + \frac{1}{q_e} \right) \tag{9}$$

Sorption energy, E, can be evaluated from K thus [55]:

$$E = \left(2\beta \right)^{-1/2} \tag{10}$$

where q_m may also symbolize the total specific micropore volume of the sorbent or the theoretical adsorption capacity.

3.3.6. Redlich–Peterson model

This model, which is employed for demonstrating adsorption equilibrium for a wide range of concentrations, has the usability for both homogeneous and heterogeneous systems because of its flexibility; this can be enlightened by following Eq. (11) [56,57]:

$$\ln \left[K_R \frac{C_e}{q_e} - 1 \right] = \ln a_R + \beta \ln C_e \tag{11}$$

β is the exponent which lies between 1 and 0.

3.4. Error function

In addition to the usual way of validating kinetics models using the linear regression method, the sum of square error (SSE), is also employed in this study to determine the best fitting kinetics and isotherms.

The error function is given by [58]:

$$\text{SSE} = \sqrt{\frac{\Sigma (q_{e\,\text{exp}} - q_{e\,\text{cal}})^2}{N}} \tag{12}$$

The number of data points was shown by N.

The results of AR88 adsorption were correlated using the six isotherm models. The fit of the model with the experimental results was evaluated using linear regression analysis, as seen in Table 1. Thus, it is noted that the R^2 obtained from the Langmuir isotherm was the highest. Such a high value indicated that the Langmuir isotherm was the best model for AR88 adsorption, suggesting monolayer adsorption on the heterogeneous surface. Similar results were found in the removal of manganese from water by electrocoagulation and removal of ciprofloxacin from water by powdered activated carbon [52,59]. Also, the error coefficient for this model is lower than other models, which confirms the results. The value of R_L is <1, indicating that the adsorption of AR88 is favorable in the study case. The $(1/n)$ value in the Freundlich isotherm model is less than unity. This means that the adsorption process is preferred, the surface is heterogeneous, and there are fewer interactions between the adsorbed ions. The values of Dubinin–Radushkevich constant and are given in Table 1. For AR88 ions adsorption, the calculated value mean adsorption energy was 0.941 kJ/mol. It exhibited that AR88 ion adsorption was physical adsorption process.

Several adsorbents from other studies were compared to the adsorbents used in this research concerning their

adsorption capacities, and the comparison is presented in Table 2.

3.5. Adsorption kinetics

The illustration of the adsorption mechanism can be carried out by fitting adsorption data. The linear pseudo-first-order rate equation could be given as Eq. (13) [60]:

$$\log\left(q_e - q_t\right) = \log q_e - \frac{K_1}{2.303}t \tag{13}$$

The pseudo-second-order equation could be expressed as Eq. (14) [61]:

$$\frac{t}{q_t} = \frac{1}{K_2 q_e^2} + \frac{t}{q_e} \tag{14}$$

Moreover, K_1 (1/h) is the rate constant of pseudo-first-order and K_2 (g/mg·h) symbolizes the rate constant of pseudo-second-order adsorption processes, respectively. The fitting curves by the pseudo-first-order model were exemplified in Fig. 7 in the supplementary data. In addition, the fitting curves by the pseudo-second-order model were documented in Fig. 8. The kinetic parameters are summarized in Table 2. R^2 values obtained were notable (higher than 0.935) at different concentrations for both models. However, comparing the theoretical and experimental q_e, revealed that there is a wide gap between the q_e values obtained from the pseudo-first-order model (2.14–24.9 mg/g) and experimental q_e values (4.975–40.19 mg/g) for all concentrations studied (Table 3). For the pseudo-second-order model, the calculated q_e values (4.26–38.73 mg/g) were in close consistency with the experimental values (Table 3).

Therefore, it was observed that the pseudo-second-order model was found to be statistically significant based on the higher values of coefficient of regression and lower values of SSE error compared to the values obtained for the pseudo-first-order model.

Following equation is related to intraparticle diffusion model [62]:

$$q_t = K_d t^{1/2} + C \tag{15}$$

Plotting q_t vs. $t^{1/2}$ gives a line; passing through the obtained line from origin illuminates that only intraparticle diffusion is the rate-limiting step. However, the lack of passing through of the line is inactive of participation of film diffusion in the process; this offers the idea of the thickness of the boundary layer. According to Fig. 9, which shows the intraparticle diffusion plots, two stages can be considered for the adsorption process, which include a quick stage at the beginning and a gradually slower stage until achieving the adsorption equilibrium over adsorption time. This shows that both intraparticle diffusion and the film diffusion control the studied process.

The Boyd plot can forecast the actual slow step, which is included in the adsorption process. Eq. (16) is related to Boyd kinetic [63]:

$$B = -0.4977 - \ln\left(1 - F\right) F = \frac{q_t}{q_0} \tag{16}$$

where q_0 is representative of the amount of studied pollutant adsorbed at infinite time (mg/g). q_t symbolizes the amount of AR88 adsorbed at any time t (min), F signifies the fraction of solute adsorbed at any time t. B shows the mathematical function of F. The Boyd plots, provided in Fig. 10, illuminate that, for all the examined dye concentrations, the plots are linear. Based on the suggestions of the Boyd plots, the

Table 1
Isotherm constants for the adsorption of AR88

Langmuir		Temkin	
q_m	91.7	A	85.45
R_L	0.526	B	0.049
R^2	0.998	R^2	0.64
SSE	0.746	SSE	1.731
Freundlich		Harkin–Jura	
K_F	10.64	A	28.61
n	3.679	B	0.784
R^2	0.924	R^2	0.895
SSE	4.848	SSE	3.741
Dubinin–Radushkevich		Redlich–Peterson	
q_m	24.85	a_R	0.486
K	0.0024	β	1.044
E	0.941	K_R	5.943
R^2	0.975	R^2	0.942
SSE	2.731	SSE	7.451

Table 2
Comparison of the adsorption capacities of dye using various adsorbents

Materials	Adsorption capacity (mg/g)	References	Materials	Adsorption capacity (mg/g)	References
MgO nanoparticles	41.2	[2]	Pine tree leaves	19.3	[16]
Lemna minor	21.2	[3]	MWCNT	71.3	[19]
Sepiolite	7.49	[11]	*Thuja orientalis*	9.21	[20]
Maghemite	13.6	[12]	Canola residues	14.2	[22]
Tea waste	16.5	[13]	AC-bagasse	17.2	[23]
Fruit waste	23.2	[14]	HDTMA-bentonite	91.7	This study

Table 3
Kinetic models and error analysis parameters for AR88 adsorption

Kinetic models	Parameters	AR88 concentration (mg/L)			
		10	25	50	100
Pseudo-first-order	$q_{e,cal}$ (mg/g)	2.141	5.676	11.89	24.95
	$q_{e,exp}$ (mg/g)	4.975	11.95	22.68	40.19
	K_1	0.0528	0.0392	0.0281	0.0214
	R^2	0.936	0.942	0.938	0.947
	SSE	11.25	9.84	12.39	7.471
Pseudo-second-order	$q_{e,cal}$ (mg/g)	4.262	10.37	21.19	38.73
	$q_{e,exp}$ (mg/g)	4.975	11.95	22.68	40.19
	K_2	0.0079	0.0066	0.0027	0.0009
	R^2	0.998	0.999	0.996	0.997
	SSE	0.974	1.182	1.721	0.928
Intraparticle diffusion	K	0.321	0.806	1.692	3.112
	C	2.022	4.463	6.851	11.18
	R^2	0.761	0.763	0.789	0.785
	SSE	8.412	7.156	9.721	5.973

external mass transfer is the rate-determining step (because the plots were linear and do not pass through the origin).

3.6. Thermodynamic studies

To demonstrate the thermodynamic behavior of AR88 ions adsorption process, thermodynamic parameters such as $\Delta G°$ as well as $\Delta S°$ and $\Delta H°$ change can be determined. Table 4 shows the changes of $\Delta S°$ and $\Delta H°$ calculated from the intercept and slope of ln$K$ against 1/T plot, respectively [63].

$$\Delta G° = RT \ln k_c \tag{17}$$

$$\ln K_c = \frac{\Delta S°}{R} - \frac{\Delta H°}{RT} \tag{18}$$

$$\Delta G° = \Delta H° - T\Delta S° \tag{19}$$

The $\Delta G°$ measures the spontaneity of the adsorption process, with a higher negative value indicating more powerfully favorable adsorption. The thermodynamic feasibility and spontaneous nature of AR88 adsorption process on HDTMA-bentonite are confirmed by the negative $\Delta G°$ values [64]. The values of $\Delta G°$ decrease from –4.45 to –10.71 kJ/mol, respectively, as the temperature, rises from 293 to 323 K (Table 3). The decline in the values of $\Delta G°$ as temperature rises shows that adsorption is less feasible at higher temperatures. The adsorption of AR88 ions was of an endothermic nature, as evidenced by the positive $\Delta H°$ values. Furthermore, the improved randomness during the AR88 adsorption at the interface of solid/solution is indicated by the positive $\Delta S°$ values (Table 4).

3.7. Regeneration studies

The adsorption of AR88 dye is a reversible process, hence the saturated HDTMA-bentonite can be regenerated and reused for adsorption. The efficiency of regenerated HDTMA-bentonite is checked by conducting the experiments at 10 mg/L of initial AR88 concentration. The regenerated HDTMA-bentonite was applied in six consecutive cycles of adsorption/desorption. The adsorption amount presented was consistent through the cycles and experienced the adsorption capacity decreased by 19.2% after six generations which suggests it may be used as a sustainable AR88 dye removal (Fig. 11).

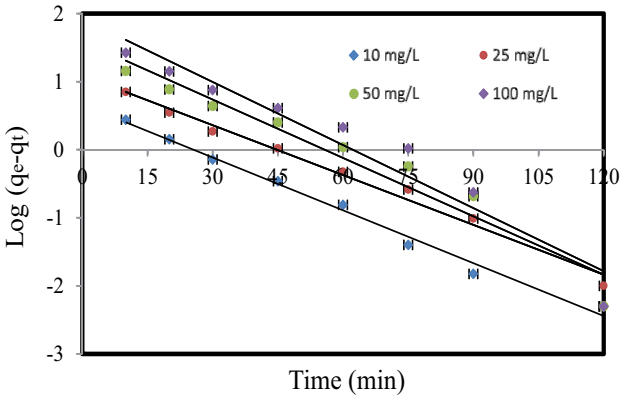

Fig. 7. Pseudo-first-order kinetics plots of AR88 adsorption onto HDTMA-bentonite.

3.8. Test with real textile industry sewage

This study was performed using synthetic wastewater, but finally a test was performed for textile wastewater with an initial COD of 620 mg/L and the results showed that after 120 min of contact time, 71% reduction in the amount of COD is observed. The experiments were performed at the optimum absorbent dose of 2 g/L at pH 5 and temperature 30°C.

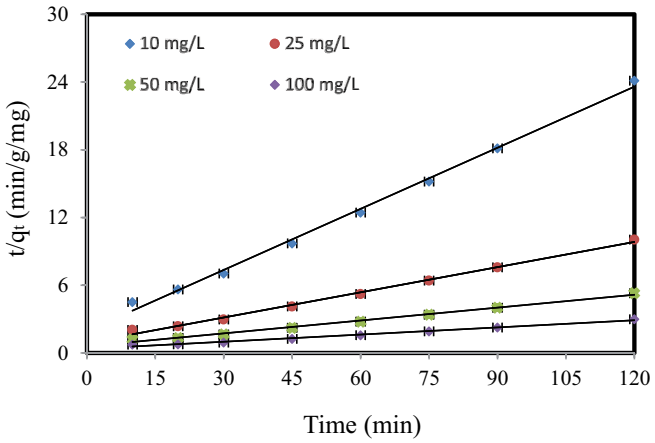

Fig. 8. Pseudo-second-order kinetics plots of AR88 adsorption onto HDTMA-bentonite.

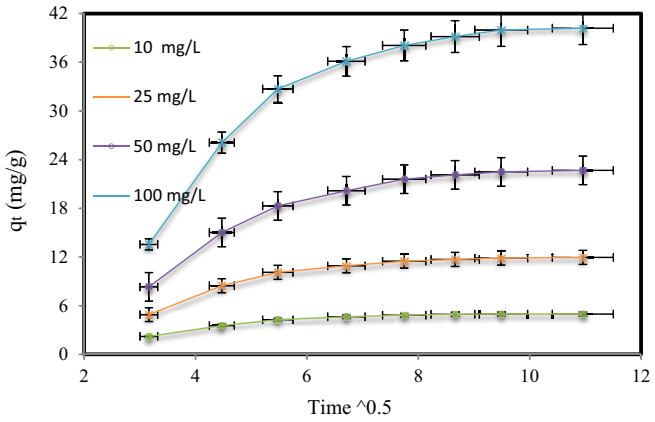

Fig. 9. Intraparticle diffusion model for the adsorption of AR88 onto HDTMA-bentonite.

Table 4
Thermodynamic parameters for the adsorption of AR88 on HDTMA-bentonite

T (K)	$\Delta G°$ (kJ/mol)	$\Delta H°$ (kJ/mol)	$\Delta S°$ (kJ/mol·K)
293	–4.45	53.2	0.189
303	–6.02		
313	–8.19		
323	–10.71		

4. Conclusion

This work focuses on the removal of AR88 using HDTMA-bentonite. The effect of different parameters was investigated in batch experiments. Thermodynamics analyses indicate that the AR88 sorption is feasible, spontaneous, and endothermic with enthalpy and entropy equal to 53.2 kJ/mol and 0.189 kJ/mol. K, respectively. Kinetic studies revealed that the adsorption process follows pseudo-second-order due to the higher regression coefficient and lower error coefficient. The optimum conditions were obtained at

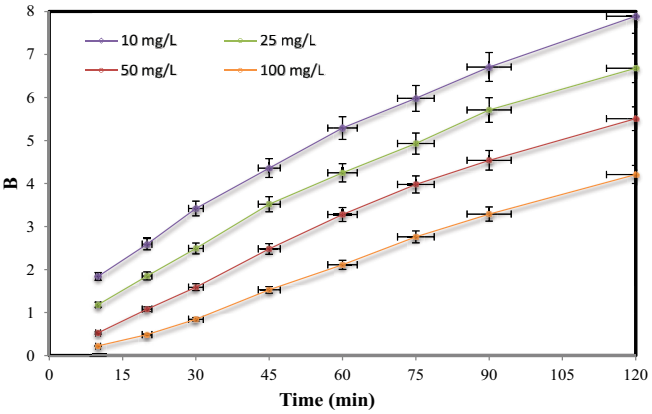

Fig. 10. Boyd plot for the adsorption of AR88 onto HDTMA-bentonite.

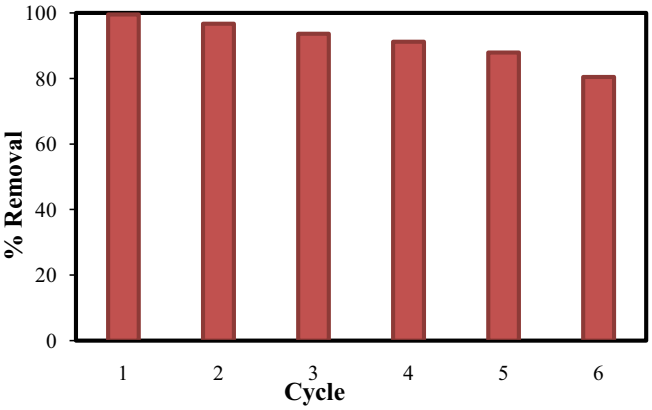

Fig. 11. Removal % of AR88 dye by regenerated HDTMA-bentonite.

AR88 concentration of 10 mg/L, HDTMA-bentonite dose 2 g, solution pH 3, equilibrium time 90 min, and temperature 30°C, giving the highest percentage of AR88 removal 99.5%. The adsorption isotherms of AR88 were also compared with popular models, and it was found that the AR88 uptake was well-described by the Langmuir model with maximum adsorption capacities of 91.7 mg/g. The adsorption study revealed that HDTMA-bentonite is an effective, promising, and highly reusable sorbent for removal contaminants like dye from wastewater with low cost.

Abbreviation and symbols

R-P	—	Redlich–Peterson
D-R	—	Dubinin–Radushkevich
PSO	—	Pseudo-second-order
PFO	—	Pseudo-first-order
IPD	—	Intraparticle diffusion
C_0	—	Initial concentration of AR88, mg/g
C_e	—	Concentration at equilibrium (after adsorption), mg/L
m	—	HDTMA-bentonite mass, g
V	—	Volume of AR88 solution, L

q_m — maximum adsorption capacity, mg/g
K_L — Langmuir constant, L/mg
n and K_F — Parameters of Freundlich model
E — Free energy of adsorption for Dubinin–Radushkevich, kJ/mol
β — Constant of Dubinin–Radushkevich isotherm, mol^2/J^2
ε — Polanyi potential corresponding to the equilibrium concentration, J/mol
R — Universal gas constant, 8.314 kJ/mol
T — Absolute temperature, K
A — Equilibrium binding constant related to the maximum binding energy, L/mg
b — Temkin constant corresponding to the sorption heat, J/mol
K_R — Displays the Redlich–Peterson constant, L/g
a_R — Indicates the Redlich–Peterson constant, L/mg
K_1 — Equilibrium rate constant for pseudo-first-order kinetics, 1/min
K_2 — Equilibrium rate constant for pseudo-second-order kinetics, g/mg·min
K_d — Intraparticle diffusion rate constant, $mg/g·min^{1/2}$

Acknowledgement

The authors are grateful to the Student research committee of Zahedan University of Medical Sciences because of supporting this research (code project: 10783).

References

[1] M. Arami, N.Y. Limaee, N.M. Mahmoodi, Evaluation of the adsorption kinetics and equilibrium for the potential removal of acid dyes using a biosorbent, Chem. Eng. J., 139 (2008) 2–10.
[2] G. Moussavi, M. Mahmoudi, Removal of azo and anthraquinone reactive dyes from industrial wastewaters using MgO nanoparticles, J. Hazard. Mater., 168 (2009) 806–812.
[3] D. Balarak, Y. Mahdavi, F.K. Mostafapour, A. Joghataei, Batch removal of Acid Blue 292 dye by biosorption onto *Lemna minor*: equilibrium and kinetic studies, J. Hum. Environ. Health Promot., 2 (2016) 9–19.
[4] C. Muthukumaran, V.M. Sivakumar, M. Thirumarimurugan, Adsorption isotherms and kinetic studies of crystal violet dye removal from aqueous solution using surfactant modified magnetic nanoadsorbent, J. Taiwan Inst. Chem. Eng., 63 (2010) 354–362.
[5] R. Kamaraj, A. Pandiarajan, S. Vasudevan, S. Vasudevan, Facile one-pot electrosynthesis of zinc hydroxide for the adsorption of hazardous 2-(2-methyl-4-chlorophenoxy) propionic acid (MCPP) from water and its modelling studies, J. Environ. Chem. Eng., 6 (2018) 2017–2026.
[6] A. Pandiarajan, R. Kamaraj, S. Vasudevan, Enhanced removal of cephalosporin based antibiotics (CBA) from water by one-pot electrosynthesized $Mg(OH)_2$: a combined theoretical and experimental study to pilot scale, New J. Chem., 41 (2017) 4518–4530.
[7] R. Kamaraj, S. Vasudevan, Facile one-pot electrosynthesis of $Al(OH)_3$ – kinetics and equilibrium modeling for adsorption of 2,4,5-trichlorophenoxyacetic acid from aqueous solution, New J. Chem., 40 (2016) 2249–2258.
[8] R. Kamaraj, D.J. Davidson, G. Sozhan, S. Vasudevan, Adsorption of 2,4-dichlorophenoxyacetic acid (2,4-D) from water by in situ generated metal hydroxides using sacrificial anodes, J. Taiwan Inst. Chem. Eng., 45 (2014) 2943–2949.
[9] R. Kamaraj, D.J. Davidson, G. Sozhan, S. Vasudevan, An in situ electrosynthesis of metal hydroxides and their application for adsorption of 4-chloro-2-methylphenoxyacetic acid (MCPA) from aqueous solution, J. Environ. Chem. Eng., 2 (2014) 2068–2077.
[10] E. Eren, O. Cubuk, H. Ciftci, B. Eren, B. Caglar, Adsorption of basic dye from aqueous solutions by modified sepiolite: equilibrium, kinetics and thermodynamics study, Desalination, 252 (2010) 88–96.
[11] A. Ozcan, A.S. Ozcan, Adsorption of Acid Red 57 from aqueous solutions onto surfactant-modified sepiolite, J. Hazard. Mater., 125 (2005) 252–259.
[12] A. Afkhami, M. Saber-Tehrani, H. Bagheri, Modified maghemite nanoparticles as an efficient adsorbent for removing some cationic dyes from aqueous solution, Desalination, 263 (2010) 240–248.
[13] M.T. Uddin, M.A. Islam, S. Mahmud, M. Rukanuzzaman, Adsorptive removal of methylene blue by tea waste, J. Hazard. Mater., 164 (2009) 53–60.
[14] F.A. Pavan, E.C. Lima, S.L.P. Dias, A.C. Mazzocato, Methylene blue biosorption from aqueous solutions by yellow passion fruit waste, J. Hazard. Mater., 150 (2008) 703–712.
[15] A. Assadi, A. Soudavari, M. Mohammadian, Comparison of electrocoagulation and chemical coagulation processes in removing Reactive red 196 from aqueous solution, J. Hum. Environ. Health Promot., 1 (2016) 172–182.
[16] F. Deniz, S. Karaman, Removal of Basic Red 46 dye from aqueous solution by pine tree leaves, Chem. Eng. J., 170 (2011) 67–74.
[17] A. Yosuf, G. Mollah, K.D. Kamol, L. David, Electrochemical treatment of Orange II dye solution-use of aluminum sacrificial electrodes and floc characterization, J. Hazard. Mater., 174 (2010) 851–858.
[18] M.T. Uddin, M.A. Islam, S. Mahmud, M. Rukanuzzaman, Adsorptive removal of methylene blue by tea waste, J. Hazard. Mater., 164 (2009) 53–60.
[19] H. Gao, S. Zhao, X. Cheng, X. Wang, L. Zheng, Removal of anionic azo dyes from aqueous solution using magnetic polymer multi-wall carbon nanotubes nanocomposite as adsorbent, Chem. Eng. J., 223 (2013) 84–90.
[20] T. Akar, A.S. Ozcan, S. Tunali, A. Ozcan, Biosorption of a textile dye (Acid Blue 40) by cone biomass of *Thuja orientalis*: estimation of equilibrium, thermodynamic and kinetic parameters, Bioresour. Technol., 99 (2008) 3057–3065.
[21] H. Gao, S. Zhao, X. Cheng, X. Wang, L. Zheng, Removal of anionic azo dyes from aqueous solution using magnetic polymer multi-wall carbon nanotubes nanocomposite as adsorbent, Chem. Eng. J., 223 (2013) 84–90.
[22] D. Balarak, J. Jaafari, G. Hassani, Y. Mahdavi, I. Tyagi, S. Agarwal, V.K. Gupta, The use of low-cost adsorbent (Canola residues) for the adsorption of methylene blue from aqueous solution: isotherm, kinetic and thermodynamic studies, Colloids Interface Sci. Commun., 7 (2015) 16–19.
[23] N.K. Amin, Removal of reactive dye from aqueous solutions by adsorption onto activated carbons prepared from sugarcane bagasse pith, Desalination, 223 (2008) 152–161.
[24] J. Galán, A. Rodríguez, J.M. Gómez, S.J. Allen, G.M. Walker, Reactive dye adsorption onto a novel mesoporous carbon, Chem. Eng. J., 219 (2013) 62–68.
[25] Z. Li, H. Hong, L. Liao, A mechanistic study of ciprofloxacin removal by kaolinite, Colloids Surf., B, 88 (2011) 339–344.
[26] S.S. Gupta, G. Bhattacharyya, Adsorption of heavy metals on kaolinite and montmorillonite: a review, Phys. Chem. Chem. Phys., 14 (2012) 6698–6723.
[27] Z. Li, R. Beachner, Z. McManama, H. Hanlie, Sorption of arsenic by surfactant-modified zeolite and kaolinite, Microporous Mesoporous Mater., 105 (2007) 291–297.
[28] M. Salman, B. El-Eswed, F. Khalili, Adsorption of humic acid on bentonite, Appl. Clay Sci., 38 (2007) 51–56.
[29] K.G. Akompie, F.A. Dawudo, Potential of a low-cost bentonite for heavy metal abstraction from binary component system, J. Basic Appl. Sci., 4 (2015) 25–28.
[30] A.S. Ozcan, B. Erdem, A. Ozcan, Adsorption of Acid blue 193 from aqueous solutions onto Na-bentonite and DTMA-bentonite, J. Colloid Interface Sci., 280 (2004) 44–54.

[31] B. Erden, A.S. Ozcan, A. Ozcan, Preparation of HDTMA-bentonite: characterization studies and its adsorption behavior toward dibenzofuran, Surf. Interface Anal., 42 (2010) 1351–1356.
[32] A. Ozcan, C. Omeroglu, Y. Erdogan, A.S. Ozcan, Modification of bentonite with a cationic surfactant: an adsorption study of textile dye Reactive blue 19, J. Hazard. Mater., 140 (2007) 173–179.
[33] Y. Zhou, X.Y. Jin, H.F. Lin, Z.L. Chen, Synthesis, Characterization and potential application of organo-bentonite in removing 2,4-DCP from industrial wastewater, Chem. Eng. J., 166 (2011) 176–183.
[34] M.A. Zazouli, J.Y. Cherati, D. Balarak, M. Ebrahimi, Y. Mahdavi, Investigating the removal rate of Acid blue 113 from aqueous solution by canola (*Brassica napus*), J. Mazand Univ. Med. Sci., 22 (2013) 70–78.
[35] P. Luo, Y. Zhao, B. Zhang, J. Liu, Y. Yang, J. Liu, Study on the adsorption of Neutral Red from aqueous solution onto halloysite nanotubes, Water Res., 44 (2010) 1489–1497.
[36] A.A. Inyinbor, F.A. Adekola, G.A. Olatunji, Kinetics, isotherms and thermodynamic modeling of liquid phase adsorption of Rhodamine B dye onto *Raphia hookerie* fruit epicarp, Water Resour. Ind., 15 (2016) 14–27.
[37] C.Y. Kuo, C.H. Wu, J.Y. Wu, Adsorption of direct dyes from aqueous solutions by carbon nanotubes: determination of equilibrium, kinetics and thermodynamics parameters, J. Colloid Interface Sci., 327 (2008) 308–315.
[38] Ö. Gök, A.S. Özcan, A. Özcan, Adsorption behavior of a textile dye of Reactive Blue 19 from aqueous solutions onto modified bentonite, Appl. Surf. Sci., 256 (2010) 5439–5443.
[39] F.B. Abdur-Rahman, M. Akter, M. Zainal Abedin, Dyes removal from textile wastewater using orange peels, Int. J. Sci. Technol. Res., 2 (2013) 47–50.
[40] B.H. Hameed, A.A. Ahmad, Batch adsorption of methylene blue from aqueous solution by garlic peel, an agricultural waste biomass, J. Hazard. Mater., 164 (2009) 870–875.
[41] T.V.N. Padmesh, K. Vijayaraghavan, G. Sekaran, M. Velan, Application of *Azolla rongpong* on biosorption of Acid Red 88, Acid green 3, Acid orange 7 and Acid blue 15 from synthetic solutions, Chem. Eng. J., 122 (2006) 55–63.
[42] H. Pekkuz, I. Uzun, F. Güzel, Kinetics and thermodynamics of the adsorption of some dyestuffs from aqueous solution by poplar sawdust, Bioresour. Technol., 99 (2008) 2009–2017.
[43] A.E.N. Azza Khaled, A. El-Sikaily, O. Abdelwahab, Treatment of artificial textile dye effluent containing Direct Yellow 12 by orange peel carbon, Desalination, 238 (2009) 210–232.
[44] G. Crini, P.M. Badot, Application of chitosan, a natural amino polysaccharide, for dye removal from aqueous solutions by adsorption processes using batch studies: A review of recent literature, Prog. Polym. Sci., 33 (2008) 399–447.
[45] E.N. El Qada, S.J. Allen, G.M. Walker, Adsorption of Methylene blue onto activated carbon produced from steam activated bituminous coal: a study of equilibrium adsorption isotherm, Chem. Eng. J., 124 (2006) 103–110.
[46] Q.U. Baocheng, Z.H. Jiti, X. Xiang, C. Zheng, Z.H. Hongxia, Z.H. Xiaobai, Adsorption behavior of azo dye CI Acid red 14 in aqueous solution on surface soils, J. Environ. Sci., 20 (2008) 704–709.
[47] D. Balarak, Y. Mahdavi, E. Bazrafshan, A.H. Mahvi, Kinetic, isotherms and thermodynamic modeling for adsorption of Acid blue 92 from aqueous solution by modified *Azolla filiculoides*, Fresenius Environ. Bull., 25 (2016) 1321–1330.
[48] P.K. Malik, Use of activated carbons prepared from sawdust and rice-husk for adsorption of acid dyes: a case study of Acid yellow 36, Dyes Pigm., 56 (2003) 239–249.
[49] M.M. Mohamed, Acid dye removal: comparison of surfactant-modified mesoporous FSM-16 with activated carbon derived from rice husk, J. Colloid Interface Sci., 272 (2004) 28–34.
[50] S.P. Moussavi, M. Fazli, Acid violet 17 dye decolonization by multi-walled carbon nanotubes from aqueous solution, J. Hum. Environ. Health Promot., 1 (2016) 110–117.
[51] M.H. Rasoulifard, N. Taheri Qazvini, E. Farhangnia, A. Heidari, M.M. Doust Mohamad, Removal of Direct yellow 9 and Reactive orange 122 from contaminated water using chitosan as a polymeric bioadsorbent by adsorption process, J. Color Sci. Technol., 4 (2010) 17–23.
[52] P. Ganesan, J. Lakshmi, G. Sozhan, S. Vasudevan, Removal of manganese from water by electrocoagulation: adsorption, kinetics and thermodynamic studies, Can. J. Chem. Eng., 91 (2013) 448–458.
[53] A. Meshkinain, B. Davoud, Y. Nastaran, Optimization of nickel oxide nanoparticle synthesis through the sol–gel method for adsorption of Penicillin G, Res. J. Chem. Environ., 25 (2021) 31–36.
[54] H. Azarpira, Y. Mahdavi, O. Khaleghi, Thermodynamic studies on the removal of metronidazole antibiotic by multi-walled carbon nanotubes, Pharm. Lett., 8 11 (2016) 107–113.
[55] M. Sillanpää, A.H. Mahvi, Adsorption of Acid orange 7 dyes from aqueous solution using polypyrrole/nanosilica composite: experimental and modelling, Int. J. Environ. Anal. Chem., (2021), doi: 10.1080/03067319.2020.1855338.
[56] T.J. Al-Musawi, N. Mengelizade, O. Al Rawi, Capacity and modeling of Acid blue 113 dye adsorption onto chitosan magnetized by Fe_2O_3 nanoparticles, J. Polym. Environ., 30 (2022) 344–359.
[57] T.J. Al-Musawi, N. Mengelizade, M. Taghavi, Activated carbon derived from *Azolla filiculoides* fern: a high-adsorption-capacity adsorbent for residual ampicillin in pharmaceutical wastewater, Biomass Convers. Biorefin., (2021), doi: 10.1007/s13399-021-01962-4.
[58] D. Balarak, M. Baniasadi, S.M. Lee, M.J. Shim, Ciprofloxacin adsorption onto *Azolla filiculoides* activated carbon from aqueous solutions, Desal. Water Treat., 218 (2021) 444–453.
[59] T.J. Al-Musawi, A.H. Mahvi, A.D. Khatibi, Effective adsorption of ciprofloxacin antibiotic using powdered activated carbon magnetized by iron(III) oxide magnetic nanoparticles, J. Porous Mater., 28 (2021) 835–852.
[60] D. Balarak, Z. Taheri, M.J. Shim, S.-M. Lee, C. Jeon, Adsorption kinetics and thermodynamics and equilibrium of ibuprofen from aqueous solutions by activated carbon prepared from *Lemna minor*, Desal. Water Treat., 215 (2021) 183–193.
[61] D. Balarak, A.H. Mahvi, M.J. Shim, S.M. Lee, Adsorption of ciprofloxacin from aqueous solution onto synthesized NiO: isotherm, kinetic and thermodynamic studies, Desal. Water Treat., 212 (2021) 390–400.
[62] A.D. Khatibi, A.H. Mahvi, N. Mengelizadeh, Adsorption–desorption of tetracycline onto molecularly imprinted polymer: isotherm, kinetics, and thermodynamics studies, Desal. Water Treat., 230 (2021) 240–251.
[63] R.A. Dyanati-Tilaki, Z. Yousefi, J. Yazdani-Cherati, The ability of *Azolla* and *Lemna minor* biomass for adsorption of phenol from aqueous solutions, J. Mazand. Univ. Med. Sci., 23 (2013) 140–146.
[64] R.A. Diyanati, Z. Yousefi, J.Y. Cherati, Investigating phenol absorption from aqueous solution by dried *Azolla*, J. Mazand. Univ. Med. Sci., 22 (2013) 13–21.